journal

J. Am. Ceram. Soc., 97 [4] 1269–1275 (2014)
DOI: 10.1111/jace.12753

Morphotropic Phase Boundary in Solution-Derived $(Bi_{0.5}Na_{0.5})_{1-x}Ba_xTiO_3$ Thin Films: Part I Crystalline Structure and Compositional Depth Profile

Dulce Pérez-Mezcua,[‡,§] Rafael Sirera,[§] Iñigo Bretos,[‡] Jesús Ricote,[‡] Ricardo Jimenez,[‡] Luis Fuentes-Cobas,[¶] Ramón Escobar-Galindo,[‡] Daniel Chateigner,[‖] and M. Lourdes Calzada[‡,†]

[‡]Consejo Superior de Investigaciones Científicas- Instituto de Ciencia de Materiales de Madrid (ICMM-CSIC), Madrid 28049, Spain

[§]Departamento de Química y Edafología, Facultad de Ciencias, Universidad de Navarra, Navarra 31008, Spain

[¶]Centro de Investigación en Materiales Avanzados, Chihuahua 31109, Mexico

[‖]Laboratoire de Cristallographie et Sciences des Matériaux (CRISMAT), Université de Caen Basse-Normandie, Caen 14050, France

In this work, ferroelectric $(Bi_{0.5}Na_{0.5})_{1-x}Ba_xTiO_3$ thin films were fabricated by chemical solution deposition (CSD) with compositions $x = 0.050$–0.150. Stoichiometric thin films (hereinafter BNBT) and others containing 10 mol% excesses of Bi^{3+} and Na^+ (BNBTxs) were spin coated onto $Pt/TiO_2/SiO_2/(100)Si$ substrates and crystallized by rapid thermal processing at 650°C for 60 s in oxygen atmosphere. Crystalline structure is studied by X-ray diffraction using Cu anode ($\lambda_{Cu} = 1.5406$ Å) and synchrotron radiation ($\lambda = 0.97354$ Å). Rietveld refinement showed the coexistence of rhombohedral/tetragonal phases in the BNBT films for x values close to those reported for $(Bi_{0.5}Na_{0.5})_{1-x}Ba_xTiO_3$ bulk ceramics. Different volume fractions of the rhombohedral/tetragonal phases are detected as a function of the Ba^{2+} content. An apparent shift of the position of the morphotropic phase boundary (MPB) is observed in the BNBTxs films. Here, the MPB region appears for nominal Ba^{2+} molar values of $x \sim 0.10$ and the experiments using a grazing-incidence synchrotron radiation indicate the existence of a crystalline phase with pyrochlore structure at the film surface. Rutherford backscattering experiments (RBS) revealed that the bismuth excess is not volatilized during the crystallization of the BNBTxs films which present inhomogeneous compositional depth profile and thick Bi_xPt bottom interfaces. The MPB BNBT films with $x \sim 0.055$ have a homogeneous compositional depth profile without appreciable bottom interfaces. Scanning electron micrographs reveal less porosity and higher grain sizes in the stoichiometric films than in those with Bi^{3+} and Na^+ excesses.

I. Introduction

Lead zirconate titanate $Pb(Zr_x,Ti_{1-x})O_3$ (PZT) is the most widely used ferroelectric material in devices such as microactuators, transducers or microsensors, due to its excellent piezoelectric properties.[1] PZT presents an enhancement of the ferro-piezoelectric properties near the morphotropic phase boundary (MPB), composition in the phase diagram where rhombohedral and tetragonal crystalline phases coexist. It has been reported that the apparent continuous phase transition through this region is mediated by intermediate phases of monoclinic symmetry,[2] which results in a high electromechanical response of the MPB-PZT materials associated with a symmetry-allowed polarization rotation.[3,4] However, new legislations enforce on alternative nonhazardous materials in contrast to the lead-based PZT. This has led to a high increase in the study of lead-free ferroelectric systems for the last years.[5,6]

Bismuth sodium titanate $(Bi_{0.5}Na_{0.5})TiO_3$ (BNT)[7] has been shown as a possible candidate to replace lead-based ferropiezoelectric materials. The crystalline structure of the pure BNT perovskite has been deeply investigated in single crystal materials. Jones and Thomas have detected cubic, rhombohedral, and tetragonal phases which belong to the space groups *Pm*3*m*, *R*3*c*, and *P*4*mm*, respectively.[8,9] Two regions of coexistence of phases are found: a rhombohedral/tetragonal region around 255°C–400°C and a tetragonal/cubic region in the range of 500°C–540°C. Recent electron-diffraction studies have shown a complex and disorder structure for BNT ceramic suggesting a random distribution of the Bi^{3+} and Na^+ A-cations, which leads to an octahedral tilt disorder and to changes in crystal symmetry, proposing the Cc symmetry as the average one obtained from X-ray diffraction measurements.[10] All of these works reveal the complexity and the controversy that exist on the BNT crystalline structure.

Although BNT shows ferroelectricity at room temperature, with a relatively large remnant polarization ($P_r \sim 38$ μC/cm^2) and high Curie temperature ($T_c \sim 320$°C),[11] the material suffers from important disadvantages for practical applications derived from its high conductivity and large coercive field. To solve these drawbacks, solid solutions of BNT with different perovskite oxides have been studied, such as BNT–$BaTiO_3$,[11,12] BNT–$BiFeO_3$,[13] BNT–$Bi_{0.5}K_{0.5}TiO_3$,[14] and BNT–$Ba_{0.5}Sr_{0.3}TiO_3$,[15] trying to decrease conductivity and coercive field of pure BNT and thus making possible the applicability of the material. Among these solid solutions, mixtures of BNT and barium titanate, $BaTiO_3$, $(Bi_{0.5}Na_{0.5})_{1-x}Ba_xTiO_3$ (BNBT), are being considered as a promising lead-free alternative to the MPB-PZT. This system also presents a rhombohedral–tetragonal MPB region, where bulk ceramics have shown enhanced dielectric, ferroelectric, and piezoelectric responses.[11,16] However, a controversy concerning the crystalline structure and the $BaTiO_3$ (BT) content of the MPB region for bulk ceramics and single crystals still exists.[17–23] Based on the variation in the electrical properties and *in situ* synchrotron diffraction analysis, the MPB region for BNBT bulk ceramics has been positioned for x between

D. Damjanovic—contributing editor

Manuscript No. 33416. Received June 24, 2013; approved November 9, 2013.
[†]Author to whom correspondence should be addressed. e-mail: lcalzada@icmm.csic.es

0.055 and 0.110, where the transition from the *R*3*c*/*R*3*m* space group to *P*4*mm* occurs.[19,20] For $x = 0.060$, an electric field-induced second-order phase transition[21] with a significant volume variation has been described.[22,23] However, recent works also indicate the existence in BNBT bulk ceramics of a *P*4*bm* relaxor phase for compositions between $x = 0.055$ and 0.080 and a *P*4*mm* ferroelectric phase for $x = 0.100$–0.110. This second MPB vanishes when an electric field is applied. These energetically close phases explain the high piezoelectric response reported for BNBT bulk materials.[24]

The fabrication of BNBT thin films is required for the integration of lead-free ferroelectric materials into complementary metal oxide semiconductors process avoiding the interfacial reactions with the substrate and the cross-contamination by elements of high volatility. BNBT solid solutions contain two high-vapor pressure elements (Bi^{3+} and Na^{+}) that can be easily lost by volatilization from the film during the crystallization annealing. This implies the need of incorporating small excesses of the volatile elements into the film to surmount the possible compositional deficiency, as the main difference with respect to the conventional processing of bulk ceramics.[25–28] For a thin-film configuration, it is expected that extrinsic and intrinsic effects should determine the composition and the crystalline structure of the BNBT perovskite in the MPB region. However, the literature concerning the study of these effects on MPB–BNBT thin films is scarce.[29–31]

This work studies the crystalline structure and compositional depth profile of solution-derived BNBT perovskite thin films on Pt-coated Si substrates. Precursor solutions with and without Bi^{3+} and Na^{+} excesses are used. $(Bi_{0.5}Na_{0.5})_{1-x}Ba_xTiO_3$ films with a wide range of nominal compositions, $0.035 \leq x \leq 0.150$, are analyzed. A shift of the MPB region is observed as a function of the nominal composition, which also affects to the compositional depth profile and microstructure of the resulting films. The optimum conditions to obtain BNBT thin films in the MPB are inferred from this study, whereby an improved dielectric, ferroelectric, and piezoelectric performance of the material is expected; which should allow the preparation of films with improved properties. These properties are shown in the Part II of this study.[32]

II. Experimental Procedure

(1) Solutions and Thin Films

Two precursor sols of $(Bi_{0.5}Na_{0.5})TiO_3$, without/with 10 mol % excess of Bi^{3+} and 10 mol% excess of Na^{+}, denoted as BNT and BNTxs, respectively, were synthesized by refluxing for 8 h in air sodium acetate tri-hydrated ($Na(OCOCH_3)3H_2O$; Aldrich, 99%), bismuth acetate ($Bi(OCOCH_3)_3$; Aldrich, 99.99%), and titanium di-isopropoxide bis-acetylacetonate ($Ti(OC_3H_7)_2(CH_3COCHCOCH_3)_2$; Aldrich, 75%) in a mixture of 1,3-propanediol, acetic acid and water.[25] The molar ratio of Ti^{4+} to any of the solvents was 1.0:10.0 and the Ti^{4+}:Na^{+}:Bi^{3+} molar ratio of the metal reagents was 2.0:1.0:1.0 for the BNT sol and 2.0:1.1:1.1 for the BNTxs sol. Distilling off the byproducts in a volume of 80 vol% of the equivalent 2-propanol contained in the sols led to orange sols with an equivalent concentration of $(Bi_{0.5}Na_{0.5})TiO_3$ of ≈0.60 mol/L.

To prepare the $BaTiO_3$ (BT) precursor solution, barium carbonate ($BaCO_3$; Alfa Aesar, 99.997%) was dissolved in propionic acid and propionic anhydride at 140°C for 2 h. Then, titanium tetra-butoxide ($Ti(O(CH_2)_3CH_3)_4$; Aldrich, 99%) and 2,4-pentadione ($C_5H_8O_2$; Aldrich, 99%) were added. Finally, the mixture was diluted with 1-butanol ($C_4H_{10}O$; Sigma-Aldrich, 99.4%) to obtain a yellow solution with an equivalent concentration of $BaTiO_3$ of 0.30 mol/L.[33]

BNT sols and BT solutions were mixed to obtain $(Bi_{0.50}Na_{0.50})_{1-x}Ba_xTiO_3$ solutions with the stoichiometric nominal compositions and with different Ba^{2+} contents ($x = 0.035$, 0.055, 0.08; $y = 0.10$). Hereinafter, the resulting precursor solutions will be denoted as BNBT3.5, BNBT5.5, BNBT8.0, and BNBT10.0. On the other hand, BNTxs sols and BT solutions were mixed to obtain $(Bi_{0.55}Na_{0.55})_{1-x}Ba_xTiO_{3.30}$ solutions containing a 10 mol% excess of Bi^{3+} and a 10 mol% excess of Na^{+}, and with different Ba^{2+} contents ($x = 0.055$, 0.100, 0.150), hereinafter BNBT5.5xs, BNBT10.0xs, and BNBT15.0xs.

Diluted solutions with dried ethanol (0.2 mol/L) were deposited onto $Pt/TiO_2/SiO_2/(100)Si$ substrates (Radiant Technologies) by spin coating at 2000 rpm for 45 s and dried at 350°C for 60 s, in a hot plate. The substrates were preannealed at 700°C for 5 min (~30°C/s, O_2). The as-deposited amorphous films were crystallized by rapid thermal processing (RTP; JetStar 100T JIPELEC) in an oxygen atmosphere at 650°C for 60 s and a heating rate of ~30°C/s. Deposition, drying and crystallization were repeated six times to obtain crystalline films with thickness between 350 and 550 nm. Films were labeled with the same names as the corresponding precursor solutions.

(2) Characterization of the Thin Films

A detailed structural analysis of the crystalline phases (rhombohedral and/or tetragonal) developed in the BNBT and BNBTxs films was carried out using a closed Eulerian goniometer equipped with a Cu anode($\lambda = 1.5406$ Å), a 120° position sensitive detector and a graphite primary monochromator. Full spectra of 120° in 2θ were collected with a regular grid of 5° × 5° in χ and ϕ, with χ from 0° to 50° and ϕ from 0° to 355°. A Rietveld refinement was carried out using these X-Ray diffraction patterns. Calculations were made with the Material Analysis Using Diffraction Package (MAUD).[34] Note that the reflections of the Pt bottom electrode at 2θ of ~40°, 47°, 68°, 81°, and 86° and signals of the rhombohedral and tetragonal crystalline phases overlap. This makes necessary the use of two different layers to perform the refinement of the experimental profiles: one layer for the perovskite (rhombohedral *R*3*m* and/or tetragonal *P*4*mm*) and another one for the Pt (100% volume fraction of cubic $F\bar{3}mm$).

Grazing-incidence scattering analysis was carried out at the beamline 11-3 of Stanford Synchrotron Radiation Lightsource (Stanford). A two-dimensional (2D) position sensitive detector calibrated with a LaB_6 standard sample, a X-ray wavelength of $\lambda = 0.97354$ Å, a sample detector distance of 180 mm, a pixel and a spot size of 0.1 mm, and incidence angles between 0.1° and 5.0° were used. Experimental patterns were obtained by integration of the Debye rings processed by the software Fit-2D and these patterns were simulated with the software Anaelu.[35,36]

For the study of the compositional depth profile of the films, Rutherford backscattering spectroscopy (RBS) experiments were performed with the 5 MV HVEE Tandetron accelerator. The RBS experiments were carried out using 2 MeV He^{+} ions and the data were acquired with a silicon surface barrier detector located at a scattering angle of 170°, with an energy resolution of 16 keV at an ion dose of 10 μC. The experimental spectra were fitted with the software RBS[37] and SIMNRA.[38]

Surface and cross-section images of the thin films were obtained by field-emission gun scanning electron microscopy (FEG-SEM; Nova Nanosem 230).

III. Experimental Results and Discussion

The special characteristics of thin films make difficult a detailed XRD structural analysis by using a conventional diffractometer with a Bragg–Brentano configuration, like that usually used to characterize powders and bulk ceramics. In fact, for thin films XRD reflections have a pronounced broadening due to the small grain size and the stresses

Table I. Crystallographic Data Calculated by X-Ray Rietveld Refinement of the Experimental XRD Patterns Measured with the Four-Circle Diffractometer, for the BNBT Thin Films

		BNBT5.5		BNBT8.0		
Crystal system	BNBT3.5 Rhombohedral	Rhombohedral	Tetragonal	Rhombohedral	Tetragonal	BNBT10.0 Tetragonal
Space group	*R*3*m*	*R*3*m*	*P*4*mm*	*R*3*m*	*P*4*mm*	*P*4*mm*
a_R(Å)/a_T (Å)	3.81668(7)	3.85711(2)	3.87076(1)	3.8532(5)	3.8681(0)	3.86840(9)
α_R(°)/c_T (Å)	89.861(1)	89.4604(6)	3.88997(2)	89.596(6)	3.8917(1)	3.8905(2)
Volume fraction (%)	99.(9)	71.(0)	28.9(7)	33.1(7)	66.(8)	99.(0)
χ^2	1.083	1.153		1.215		1.165

Table II. Crystallographic Data Calculated by X-Ray Rietveld Refinement of the Experimental XRD Patterns Measured with the Four-Circle Diffractometer, for the BNBTxs Thin Films

		BNBT10.0xs		
Crystal system	BNBT5.5xs Rhombohedral	Rhombohedral	Tetragonal	BNBT15.0xs Tetragonal
Space group	*R*3*m*	*R*3*m*	*P*4*mm*	*P*4*mm*
a_R(Å)/a_T (Å)	3.8630(0)	3.8681(5)	3.8732(9)	3.868(5)
α_R(°)/c_T (Å)	89.498(8)	89.61(6)	3.8947(8)	3.888(9)
Volume fraction (%)	99.(0)	82.(4)	17.(5)	99.(4)
χ^2	1.180	1.162		1.145

induced by the substrate. Besides, some peaks from the substrate can appear overlapped to those of the crystalline film. Therefore, the analysis of the films included in this work has been carried out using a four-circle diffractometer with a Cu anode (λ_{Cu} = 1.5406 Å) and grazing-incidence X-ray synchrotron radiation scattering (λ = 0.9797 Å).

The Rietveld analysis of the XRD experimental data measured with the four-circle diffractometer reveals important information about the crystalline structure of the films derived from the BNBT and BNBTxs solutions. Crystalline structures of the BNBT bulk ceramics are taken as references for the refinement. Therefore, *R*3*m* rhombohedral and *P*4*mm* tetragonal[19,23] space groups are simultaneously used for fitting the experimental data. The calculated cell parameters, volume fraction of both crystalline structures and goodness-of-fit (chi squared, χ^2) are given in Tables I and II. Lattice parameters for the films are of the same order as those reported for their bulk counterparts.[19,23] In the case of the BNBT films, the crystalline structure of the BNBT3.5 film is fitted to a rhombohedral phase, whereas that of the BNBT10.0 film fits to a tetragonal structure. We find the crystalline structure of the BNBT5.5 film is well fitted to a mixture of the rhombohedral and tetragonal phases, being larger the volume fraction of the former one, ~70%; this is close to a recent work reported for bulk ceramics.[21] The BNBT8.0 film also exhibits both rhombohedral and tetragonal phases, but in this case the volume fraction of the tetragonal phase is larger, ~67%. The BNBTxs films show a similar evolution of the crystalline phases, but now the MPB seems to be shifted toward larger contents of BT. Thus, the XRD pattern of the BNBT10.0xs shows the coexistence of rhombohedral and tetragonal phases, obtaining a ~82% volume fraction of the former one. For the BNBT5.5xs film, a good fitting is obtained for a rhombohedral phase, whereas the experimental profile for the BNBT15.0xs film denotes the presence of a tetragonal structure.

Figure 1 shows the experimental and calculated profiles by Rietveld analysis from the XRD data of the BNBT5.5 and BNBT10.0xs thin films, compositions which are in the MPB region according to the results of Tables I and II. Note that the (111) and (200) reflections of the Pt bottom electrode at $2\theta \sim 40°$ and $2\theta \sim 47°$, respectively, and the (111)T, (111)/($1\bar{1}1$)R as well as (002)/(200)T, (200)R reflections of the rhombohedral (R) and tetragonal (T) crystalline phases overlap. This made necessary the use of a Pt layer for the adjustment of the profiles, as it has been already noted in Section II*(2)*.

Reflections corresponding to the perovskite structure are observed in both films without the detection by XRD of secondary phases. A good fitting for the BNBT and BNBTxs films between the experimental and calculated profiles was completed, when coexistence of the rhombohedral and tetragonal phases is assumed for some of the compositions of the films, which is distinctive of a MPB region. This region is around 5.5%–8.0% molar ratio of BT for the BNBT films, which is in agreement with data reported for bulk ceramics.[19] However, the MPB shifts toward higher nominal values of BT (around 10.0 mol% BT) in the case of the BNBTxs films prepared with Bi^{3+} and Na^+ excesses. This "apparent" change in the MPB position toward a larger amount of BT incorporated into the BNBT solid solution when Bi^{3+} and Na^+ excesses are used has been previously reported for these films prepared by both chemical and physic methods.[25–31] This would indicate that the excesses added to the system are not completely lost by volatilization during the crystallization annealing, thus remaining into the final composition of the film. These excesses might be incorporated into the BNT perovskite. Then, Ti ions should be transferred from the BT composition to the BNT perovskite, thus leaving free BaO. The result is an "apparent" movement of the MPB, but the true scenario is that the MPB in these BNBTxs films should be close to that observed for the BNBT films without excesses, but now free BaO should appear in the BNBTxs films. If only a partial incorporation of the Bi^{3+} and Na^+ excesses into the BNT perovskite structure is produced, then, in addition to BaO, Bi_2O_3, and Na_2O residuals not lost by volatilization should be present in the film, as well as secondary phases resulting from the possible combination of these oxides.

To analyze in deep the crystalline structure of films prepared from solutions with Bi^{3+} and Na^+ excesses and thus be able to explain the apparent shift of the MPB region in these films, the BNBT10.0xs film has been characterized by grazing-incidence X-ray synchrotron radiation scattering (Fig. 2). Two different 2D experimental patterns of this film are shown in Fig. 2, obtained with low [penetration depth ~70 nm, Fig. 2(a)] and high [penetration depth ~200 nm, Fig. 2(b)] grazing incidence angles. Note that a characteristic

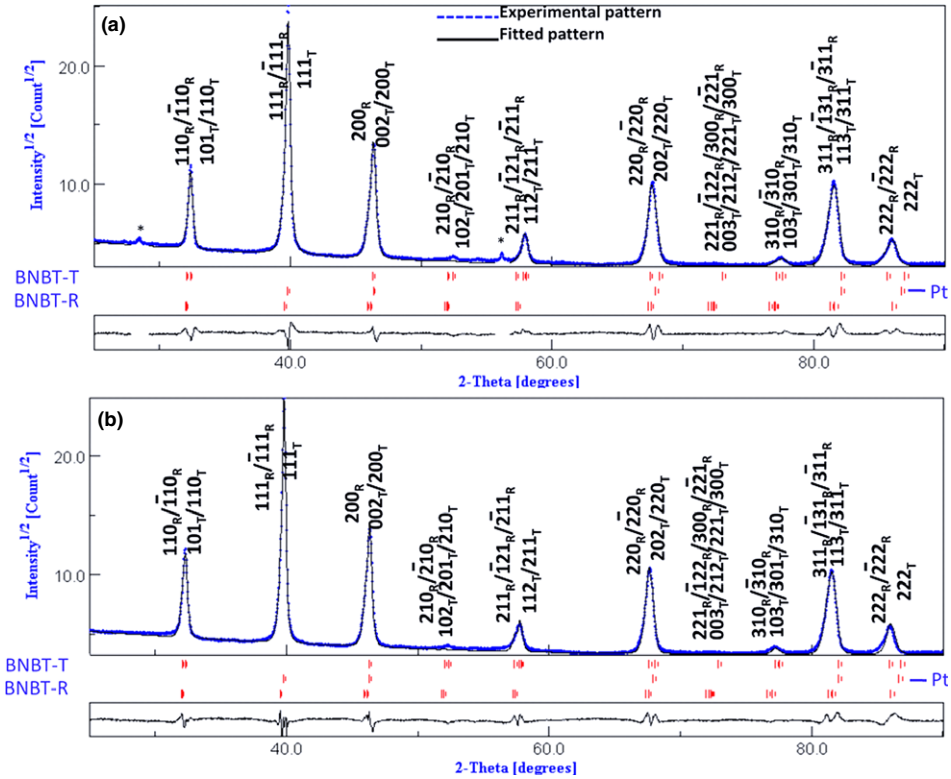

Fig. 1. Experimental (blue dotted line) and fitted (black solid line) XRD patterns of the (a) BNBT5.5 and (b) BNBT10.0xs thin films. *Indicates reflections of the silicon substrate, only observed for some of the sample orientations where the diagrams were acquired. Although there is no overlap between silicon and perovskite reflections, intervals around ~28° and ~56° (2θ) were not indexed. R and T indicate rhombohedral and tetragonal phase, respectively.

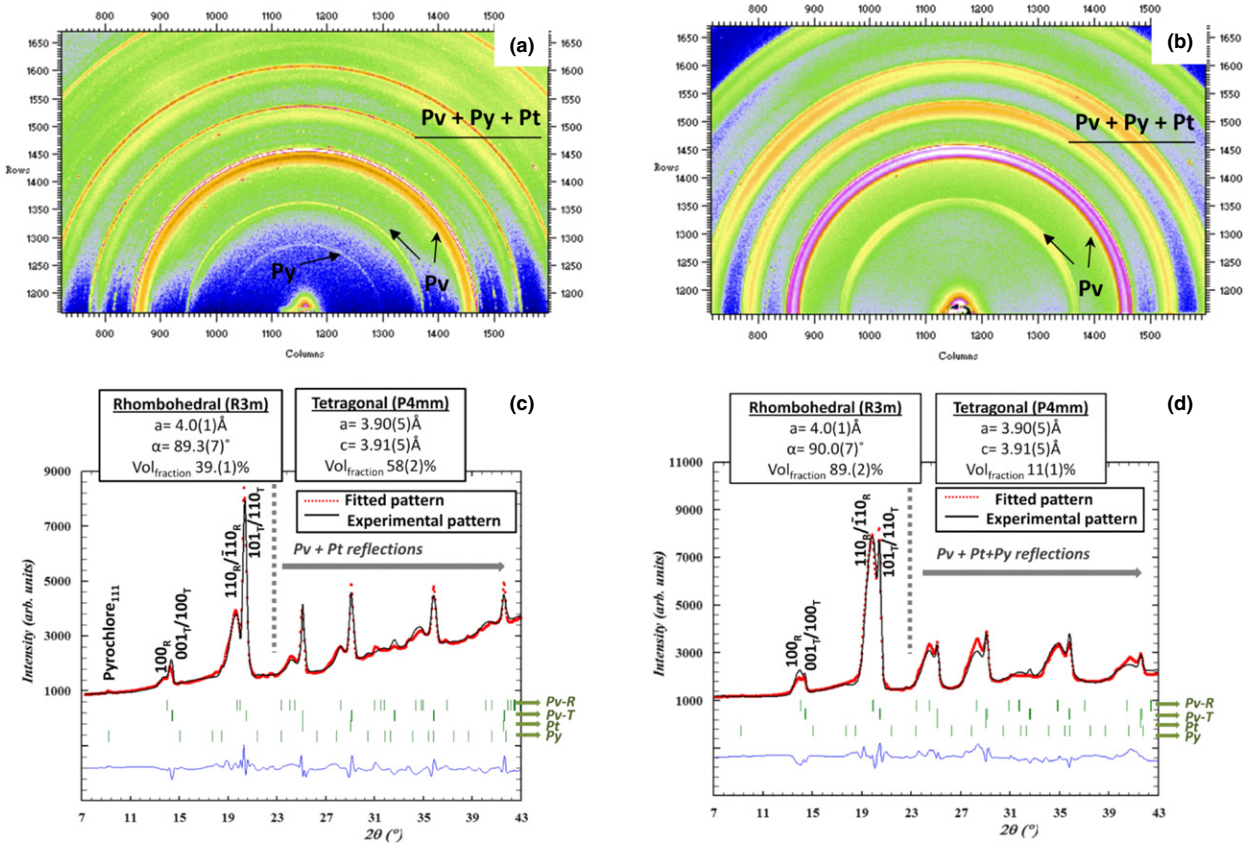

Fig. 2. Grazing-incidence X-ray syncrotron radiation scattering of the BNBT10.0xs thin film. 2D diffraction patterns using a incidence angle of: (a) 0.05° and (b) 0.15° The corresponding 1D patterns, (c) and (d), were obtained by azimuthal angle integration of the 2D patterns (black solid line) and the fitted patterns (red dotted line) were calculated using the software Anaelu.[35,36] Pt, Pv, and Py indicate platinum, perovskite phase and pyrochlore phase, respectively.

Debye ring associated with a pyrochlore structure, $Bi_2Ti_2O_7$ $Fd\bar{3}m$ (JCPDS 32- 118), is identified in the 2D pattern obtained with an incidence angle of 0.05°, which does not appear in the pattern measured with a higher incidence angle of 0.15°. This would indicate the presence of this secondary phase at the top surface of the film, but not in the bulk. On the other hand, the splitting of the peaks assigned to the *R*3*m* and *P*4*mm* phases, which is not possible to be observed in the analysis of the films with the four-circle diffractometer, is now detected in the synchrotron radiation patterns. The (111)T and (111)/(1$\bar{1}$1) R reflections at 2θ values around 25° as well as (200)/(002)T and (200)R at around 29° are very close. Besides, these peaks show a large broadening produced by the small grain size and large stresses characteristic of thin films. This makes the separation of these reflections difficult. In addition, peaks recorded at 2θ values higher than 27° cannot be analyzed for these film samples due to the overlapping with the reflections associated with the Pt bottom electrode. In spite of this, the X-ray synchrotron radiation patterns of Fig. 2 could be fitted to a rhombohedral and a tetragonal phase, *R*3*m* and *P*4*mm* space groups, respectively [Figs. 2(c) and (d)], taking into account the refinement done with the MAUD program from the XRD experimental data of Tables I and II and those results reported in the literature.[19,34,39,40] The larger broadening of the peaks associated with the R phase than to the T one should be ascribed to smaller crystallite size and larger cell strains in the former than in the latter. These results support the possible existence of a mixture of the tetragonal and rhombohedral crystalline phases. The calculated lattice parameters indicated in the Fig. 2 are close to values shown in the Table II. Similar volume fractions referred to the bulk film are also calculated for both crystalline structures; ~89% of rhombohedral phase and ~11% of tetragonal one. However, these values change at the surface of the film with a higher volume fraction of tetragonal phase than rhombohedral one; ~58% and ~39%, respectively. The observation of a pyrochlore crystalline structure at the film surface and the larger content of a tetragonal phase here than in the bulk film could be related to the volatilization of the Bi^{3+} and Na^{+} from the film surface.

Therefore, X-ray diffraction analysis of the films carried out by synchrotron radiation scattering shows differences in their crystalline structure from the top surface to the bulk film. To confirm possible compositional changes associated with these differences in crystalline structure, RBS has been used to determine variations in the compositional depth profiles of the films. These RBS experiments have been carried out in the BNBT5.5 and BNBT10.0xs thin films, both in the MPB region. As an example, the experimental and fitted RBS spectra of the BNBT5.5 sample are displayed in Fig. 3(a) together with the individual contribution of the different elements present in the film. Despite the complexity of the sample, a precise fitting of the experimental data was obtained using a multilayer approximation to describe the structure of the film.

Figure 3(b) shows the comparison between the experimental RBS spectra of the BNBT5.5 and BNBT10.0xs films. Two major differences are observed related to (i) the total thickness of the film and (ii) the quality of the film/Pt-coated substrate interface. Assuming the theoretical density of the

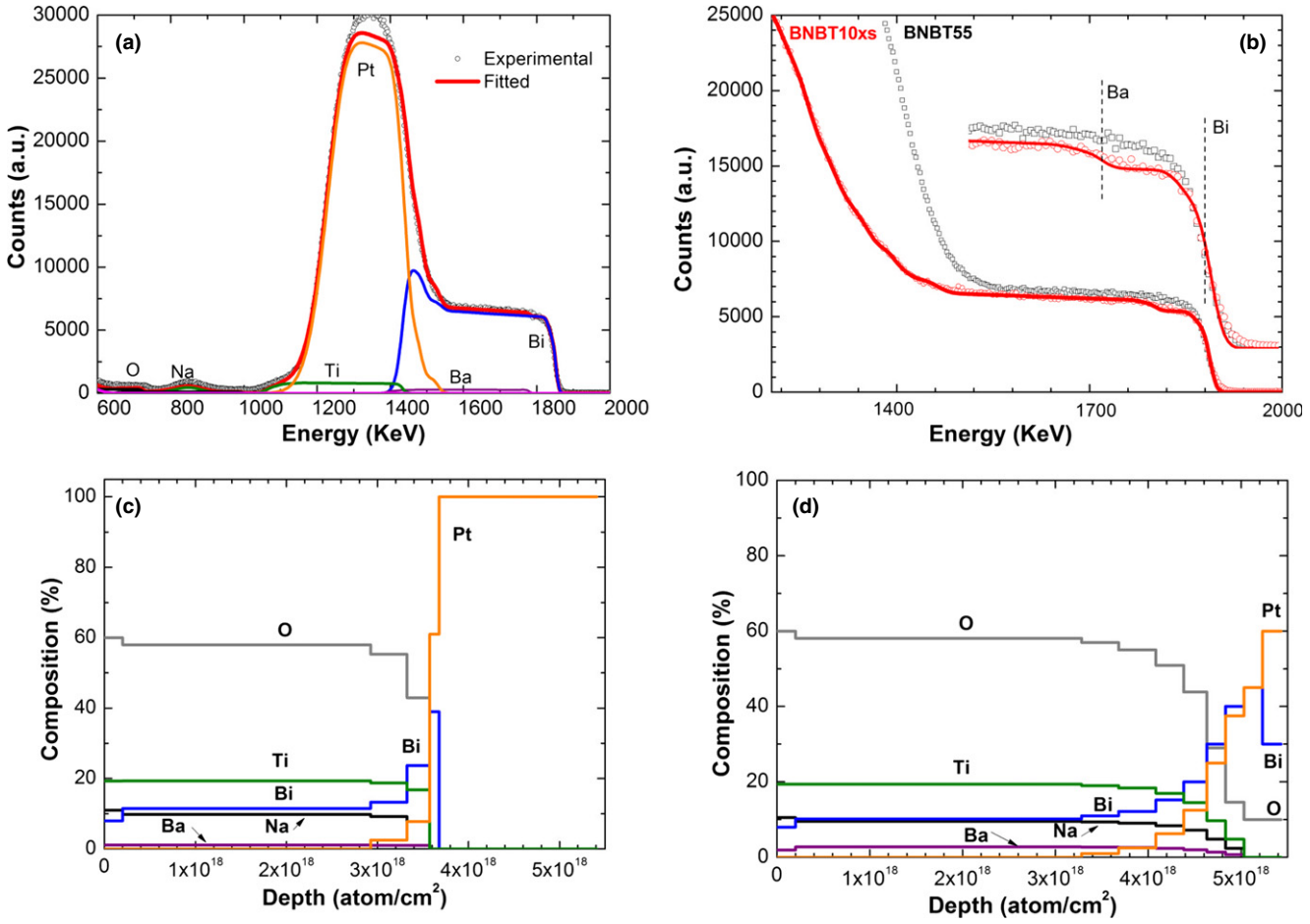

Fig. 3. (a) Rutherford backscattering experiments (RBS) experimental and fitted spectra of the BNBT5.5 film. The contributions of the elemental spectra are also displayed. (b) Comparison of the RBS spectra obtained for the BNBT5.5 and BNBT10.0xs films. In the inset, a zoom of the 1600–2000 keV region is shown, where the surface Bi and Ba are indicated by dotted vertical lines. The concentration depth profiles of the different cations forming the perovskite films are plotted for the (c) BNBT5.5 and (d) BNBT10.0xs thin films.

$(Bi_{0.5}Na_{0.5})TiO_3$ perovskite (5.92 g cm^{-3}),[41] the total thickness of the BNBT5.5 and BNBT10.0xs films was found to be of ~350 ± 5 nm and ~400 ± 5 nm, respectively. These thicknesses will be later compared to the ones measured by FEG-SEM observations and related to changes in the bulk density of the films. Besides, it is worth noting the difference in the slopes of the spectra recorded at energies below 1500 keV, this is a clear indication of the formation of an interface by the reaction between the film and the Pt-coated Si substrate. The interface was found to be unambiguously thicker for the BNBT10.0xs film. Finally, a zoom of the RBS spectra in the 1600–2000 keV region is shown in the inset of Fig. 3(b), to denote the small differences detected in the stoichiometry of the films. For example, changes of ~1 at.% (close to the RBS detection limit) on the bismuth and barium concentration in the films can be assessed due to the large cross section of helium ions with these particular elements.

For both samples, a good matching between experimental and fitted RBS spectra was completed assuming three different compositional zones [Figs. 3(c) and (d)]; (i) a top surface deficient in bismuth, (ii) a bulk film with the nominal composition of the perovskite, and (iii) an interface of reaction between the bulk film and the Pt bottom electrode. A very thin top deficient bismuth surface (~3%) was found for both films. This is produced by volatilization of this element at the film surface. It is also expected a sodium deficiency here because of its low melting point; however, the low atomic number of this element prevented its detection by RBS. The bulk films exhibit a nominal composition of $(Bi_{0.5}Na_{0.5})_{0.945}$-$Ba_{0.055}TiO_3$ for the BNBT5.5 film and of $Bi_{0.55}Na0_{.55})_{0.900}$-$Ba_{0.100}TiO_3$ for the BNBT10.0xs film, and a thickness of ~325 and ~375 nm for the former and later, respectively. The theoretical density of the $(Bi_{0.5}Na_{0.5})TiO_3$ perovskite was used for the calculation of the film thickness. Simulation of both films shows a large difference just at the bottom interface between the perovskite film and the Pt electrode. Whereas the BNBT5.5 film has an abrupt interface, what the BNBT10.0xs film shows is a progressive increase in the Bi_xPt content in the proximity of the platinum.[42] This interface is significantly thick for the BNBT10.0xs film (~40%), where a pure platinum layer can never be simulated.

Therefore, according to this RBS compositional depth profile study, the BNBT5.5 film shows a thin bismuth-deficient top surface, a ~325-nm-thick bulk film with the stoichiometric perovskite composition and an abrupt Pt-film interface. The BNBT10.0xs film shows a similar thin bismuth-deficient top surface, followed by a ~375-nm-thick bulk film with the nominal composition containing the added Bi^{3+} and Na^+ excesses, and a thick Bi_xPt interface. The presence of a Bi^{3+}-deficient surface layer in the BNBT10.0xs film could explain the presence of the pyrochlore secondary phase detected by synchrotron radiation at the surface of the BNBTxs10.0 thin film. The formation of this secondary phase together with the observation of a larger volume fraction of the tetragonal crystalline structure with respect to the rhombohedral one at the surface of the BNBT10.0xs film would be in agreement with the small loss of bismuth measured. Concerning the thickness of the film, FEG-SEM cross-section images resulted in average thicknesses of ~340 and ~550 nm for the BNBT5.5 and BNBT10.0xs films, respectively [see Figs. 4(a) and (b)]. Comparing these values to those calculated from the RBS simulations (BNBT5.5 ~350 nm and BNBT10.0xs ~400 nm), a close agreement is observed for the BNB5.5 film (only a ~3% of deviation), whereas a large deviation occurs for the BNBT10.0xs one (~25%). This difference would be related to changes in the bulk density of the film due to the larger porosity of the BNBT10.0xs film, as micrographs in Fig. 4(b) show, or to the existence of nondetected secondary phases. Note that the FEG-SEM plan view of the BNBT5.5 film [Fig. 4(a)] presents a homogenous microstructure with cohesive grains. However, the bulk of the BNBT10.0xs film [Fig. 4(b)] seems to be denser than its surface. This could be associated with the crystalline structure and compositional results obtained by grazing-incidence synchrotron radiation and RBS. Assuming the thickness of the film to be of 550 nm (as measured by SEM), a density of ~4.3 g cm^{-3} is obtained after the RBS fitting, thus with a calculated porosity of 25%–30%.

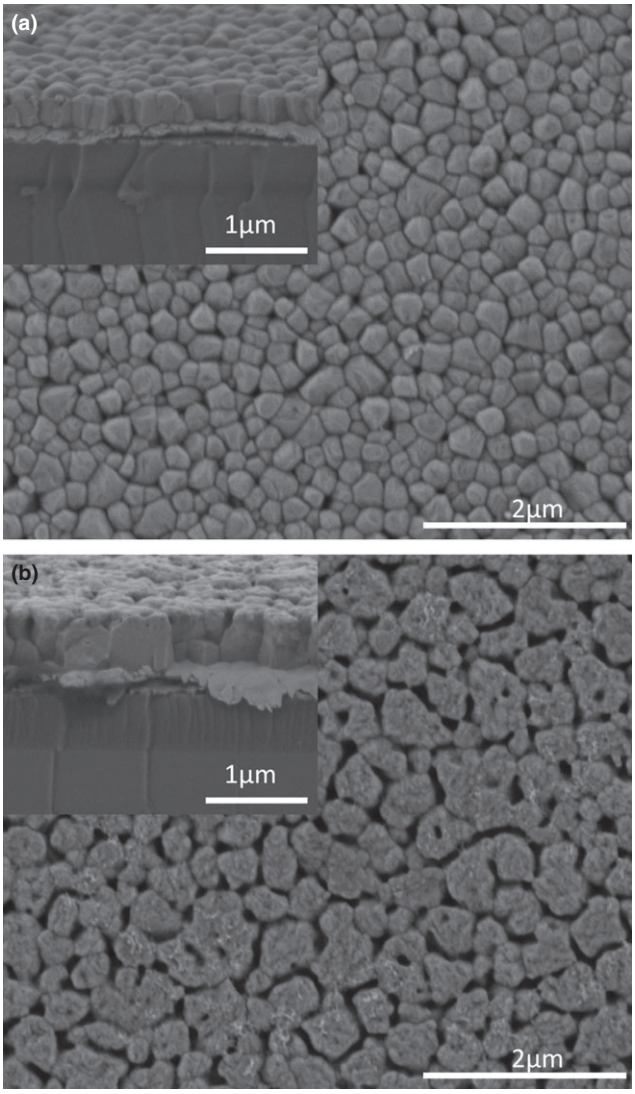

Fig. 4. Field emission gun scanning electron microscopy micrographs (cross sections and plane view) of (a) BNBT5.5 and (b) BNBT10.0xs thin films.

From the results of this work, we can hypothesize that the functional properties of these films should be enhanced in those with compositions in the MPB region, 5.5%–8.0% molar ratio of BT for the BNBT films. The BNBTxs films, containing Bi^{3+} and Na^+ excesses, show an "apparent" shift of the MPB region, observing a mixture of rhombohedral and tetragonal phases for nominal molar values of $x \sim 10.0\%$. A superior performance is expected for the MPB–BNBT films, as a homogeneous compositional profile is observed by RBS with abrupt film–substrate interfaces. On the contrary, the MPB–BNBTxs films, which show porosity, a secondary pyrochlore phase, and a large amount of the tetragonal phase at the surface exhibit, in addition, an inhomogeneous compositional depth profile and thick Bi_xPt bottom interfaces,[42] all of these probably ascribed to a nonuniform distribution of the A-cations in the perovskite structure. These structural and compositional characteristics of these films should affect the ferroelectric response of the material.[32]

IV. Conclusions

1. The MPB of solution-derived $(Bi_{0.5}Na_{0.5})_{1-x}Ba_xTiO_3$ (BNBT) thin films is located in the range of $0.055 < x < 0.080$ in accordance with most works reported for bulk ceramics of these compositions.
2. For BNBTxs films containing Bi^{3+} and Na^+ excesses, the MPB is observed close to nominal values of $x \approx 0.10$. This suggests that the Bi^{3+} and Na^+ excesses, to a large extent, remain in the bulk film total or partially incorporated into the A-sites of the perovskite. This would result in the transfer of Ti ions from $BaTiO_3$ to $(Bi_{0.5}Na_{0.5})TiO_3$, thus resulting in an "apparent" but not true movement of the MPB, in presence of free BaO and in the formation of secondary phases and interfaces.
3. According to these results, the use of the volatile element excesses within the processing of solution-derived BNBT thin films is, in principle, not required with the processing conditions here used to achieve crystalline perovskite thin films in the proximity of the MPB with homogeneous compositional profiles.

Acknowledgments

This work was financed by Spanish Project MAT2010-15365. D. Pérez-Mezcua acknowledges the financial support of the FPU Spanish program (AP2012-0639). Dr I. Bretos is grateful for the financial support of the Juan de la Cierva Spanish program. Dr R. Escobar Galindo acknowledges support through Ramon y Cajal programme (RyC2007-0026). Synchrotron studies were carried out at the Stanford Synchrotron Radiation Lightsource, a national user facility operated by Stanford University on behalf of the U.S. Department of Energy, Office of Basic Energy Sciences. Support to this activity from Project CONACYT-CNPQ 174391 "Nanoestructured Multiferroics" is recognized.

References

[1]D. Damjanovic, "Ferroelectric, Dielectric and Piezoelectric Properties of Ferroelectric Thin Films and Ceramics," *Rep. Prog. Phys.*, **61**, 1267–324 (1998).
[2]B. Noheda, D. E. Cox, G. Shirane, J. A. Gonzalo, L. E. Cross, and S. E. Park, "A Monoclinic Ferroelectric Phase in the $Pb((Zr_{1-x}Ti_x)O_3$ Solid Solution," *Appl. Phys. Lett.*, **74**, 2059–61 (1991).
[3]H. Fu and R. E. Cohen, "Polarization Rotation Mechanism for Ultrahigh Electromechanical Response in Single-Crystal Piezoelectrics," *Nature*, **403**, 281–3 (2000).
[4]R. E. Cohen, "Relaxors Go Critical,"*Nature*, **441**, 941–2 (2006).
[5]M. D. Maeder, D. Damjanovic, and N. Setter, "Lead- Free Piezoelectric Materials," *J. Electroceram.*, **13**, 385–92 (2004).
[6]J. Rödel, W. Jo, K. Seifert, E. Antón, T. Granzow, and D. Damjanovic, "Perspectives on the Development of Lead-Free Piezoceramics," *J. Am. Ceram. Soc.*, **92**, 1153–77 (2009).
[7]V. A. Isupov, "Ferroelectric $Na_{0.5}Bi_{0.5}TiO_3$ and $K_{0.5}Bi_{0.5}TiO_3$ Perovskite and Their Solid Solutions," *Ferroelectrics*, **315**, 123–47 (2005).
[8]G. O. Jones and P. A. Thomas, "Investigation of the Structure and Phase Transitions in the Novel A-Site Subtituted Distorted Perovskite Compound $Na_{0.5}Bi_{0.5}TiO_3$," *Acta Crystallogr. Sect. B: Struct. Sci.*, **58**, 168–78 (2002).
[9]G. O. Jones and P. A. Thomas, "The Tetragonal Phase of $Na_{0.5}Bi_{0.5}TiO_3$-a new Variant of the Perovskite Structure," *Acta Crystallogr. Sect. B: Struct. Sci.*, **56**, 426–30 (2000).
[10]I. Levin and M. Reany, "Nano- and Mesoscale Structure of Na ½ Bi ½ TiO_3: A TEM Perspective," *Adv. Funct. Mater.*, **22**, 3445–52 (2012).
[11]T. Takenaka and K. Sakata, "Dielectric, Piezoelectric and Pyroelectric Properties of $(Na,Bi)_{1/2}TiO_3$- Based Ceramics," *Ferroelectrics*, **95**, 153–6 (1989).
[12]C. Xu, D. Lin, and K. W. Kwok, "Structure, Electrical Properties and Depoling Temperature of $Bi_{1/2}Na_{1/2}TiO_3$–$BaTiO_3$ Lead- Free Piezoelectric Ceramics," *Solid State Sci.*, **10**, 934–40 (2008).
[13]V. Dorcet, P. Marchet, and G. Trolliard, "Structural and Dielectric Studies of the $Na_{0.5}Bi_{0.5}TiO_3$–$BiFeO_3$ System," *J. Eur. Ceram. Soc.*, **27**, 4371–4 (2007).
[14]M. Otonicar, S. D. Skapin, M. Spreitzer, and D. Suvorov, "Compositional Range and Electrical Properties of the Morphotropic Phase Boundary in the $Na_{0.5}Bi_{0.5}TiO_3$–$K_{0.5}Bi_{0.5}TiO_3$ System," *J. Eur. Ceram. Soc.*, **30**, 971–9 (2010).
[15]W. C. Lee, C. Y. Huang, L. K. Tsao, and Y. C. Wu, "Crystal Structure, Dielectric, Ferroelectric Properties of $Bi_{1/2}Na_{1/2}TiO_3$–$(Ba,Sr)TiO_3$ Piezoelectric Ceramics," *J. Alloy. Compd.*, **492**, 307–12 (2010).
[16]T. Takenaka, K. I. Maruyama, and K. Sakata, "$Bi_{1/2}Na_{1/2}TiO_3$–$BaTiO_3$ System for Lead-Free Piezoelectric Ceramics," *Jpn. J. Appl. Phys.*, **30**, 2236–9 (1991).
[17]D. Rout, K. S. Moon, S. Rao, and S. J. Kang, "Study of the Morphotropic Phase Boundary in the Lead-Free $Na_{1/2}Bi_{1/2}TiO_3$–$BaTiO_3$ System by Raman Spectroscopy," *J. Ceram. Soc. Jpn.*, **117**, 797–800 (2009).
[18]P. A. Thomas, S. Trujillo, M. Bourdard, S. Gorfman, and J. Kreisel, "Diffuse X- ray Scattering in the Lead- Free Piezoelectric Crystals $Na_{1/2}Bi_{1/2}TiO_3$ and Ba- Doped $Ba_{1/2}Bi_{1/2}TiO_3$," *Solid State Science*, **12**, 311–7 (2010).
[19]W. Jo, J. E. Daniel, J. L. Jones, X. Tan, P. A. Thomas, D. Damjanovic, and J. Rödel, "Evolving Morphotropic Phase Boundary of $Bi_{1/2}Na_{1/2}TiO_3$–$BaTiO_3$ Piezoceramics," *J. Appl. Phys.*, **109**, 014110 (2011).
[20]W. Jo, S. Schaab, E. Sapper, L. A. Schmitt, H. J. Kleebe, A. J. Bell, and J. Rödel, "On the Phase Identity and its Thermal Evolution of the Lead Free $Bi_{1/2}Na_{1/2}TiO_3$-$BaTiO_3$," *J. Appl. Phys.*, **110**, 074106 (2011).
[21]W. Jo, J. Daniels, D. Damjanovic, W. Kleemann, and J. Rödel, "Two-Stage Processes of Electrically Induced-Ferroelectric to Relaxor Transition in $0.94(Bi_{1/2}Na_{1/2})TiO_3$–$0.06BaTiO_3$," *Appl. Phys. Lett.*, **102**, 192903 (2013).
[22]W. Jo and J. Rödel, "Electric-Field-Induced Volume Change and Room Temperature Phase Stability of $(Bi_{1/2}Na_{1/2})TiO_3$-*x*mol% $BaTiO_3$ Piezoceramics," *Appl. Phys. Lett.*, **99**, 042901 (2011).
[23]H. Simons, J. E. Daniels, J. Glaum, A. J. Studer, J. L. Jones, and M. Hoffman, "Origin of Large Recoverable Strain in $0.94(Bi_{0.5}Na_{0.5})TiO_3-0.06BaTiO_3$ Near the Ferroelectric-Relaxor Transition," *Appl. Phys. Lett.*, **102**, 062902 (2013).
[24]M. Cheng, G. Hanzheng, P. B. Scott, and T. Xiaoli, "Creation and Destruction of Morphotropic Phase Boundaries Through Electrical Poling: A Case Study of Lead-Free $Bi_{1/2}Na_{1/2}TiO_3$-$BaTiO_3$ Piezoelectrics," *Phys. Rev. Lett.*, **109**, 107602 (2012).
[25]D. Alonso- Sanjosé, R. Jiménez, I. Bretos, and M. L. Calzada, "Lead-Free $Bi_{1/2}Na_{1/2}TiO_3$-$BaTiO_3$ Ferroelectric Thin Films in the Morphotropic Phase Boundary Composition: Solution Processing and Properties," *J. Am. Ceram. Soc.*, **92** [10] 2218–25 (2009).
[26]M. Cernea, L. Trupina, C. Dragoi, B. S. Vasile, and R. Trusca, "Structural and Piezoelectric Characteristics of BNT–BT0.05 Thin Films Processed by sol–Gel Technique," *J. Alloy. Compd.*, **515**, 166–70 (2012).
[27]Z. H. Zhou, J. M. Xue, W. Z. Li, and J. Wang, "Ferroelectric and Electrical Behavior of $(Na_{0.5}Bi_{0.5})TiO_3$ Thin Films," *Appl. Phys. Lett.*, **85**, 804–6 (2004).
[28]C. Dragoi, M. Cernea, and L. Trupina, "Lead- free ferroelectric $BaTiO_3$ doped-$Na_{0.5}$ $Bi_{0.5}TiO_3$ thin films processed by pulsed laser deposition technique," *Appl. Surf. Sci.*, **257**, 9600–5 (2011).
[29]I. Bretos, D. Alonso- Sanjosé, R. Jiménez, J. Ricote, and M. L. Calzada, "Evidence of Morphotropic Phase Boundary Displacement in Lead- Free $(Na_{0.5}Bi_{0.5})_{1-x}Ba_xTiO_3$ Polycrystalline Thin Films," *Mater. Lett.*, **65**, 2714–6 (2011).
[30]N. Scarisoreanu, F. Craciun, V. Ion, S. Birjega, and M. Dinescu, "Structural and Electrical Characterization of Lead-Free Ferroelectric $(Na_{0.5}Bi_{0.5})TiO_3$-$BaTiO_3$ Thin Films Obtained by PLD and RF-PLD," *Appl. Surf. Sci.*, **254**, 1292–7 (2007).
[31]D. Z. Zhang, X. J. Zheng, X. Feng, T. Zhang, J. Sun, S. H. Dai, L. J. Gong, Y. Q. Gong, L. He, Z. Zhu, J. Huang, and X. Xu, "Ferro-Piezoelectric Properties of $0.94(Na_{0.5}Bi_{0.5})TiO_3-0.06BaTiO_3$ Thin Film Prepared by Metal-Organic Decomposition," *Appl. Phys. Lett.*, **504**, 129–33 (2010).
[32]A. Perez-Rivero1, J. Ricote, I. Bretos, M. L. Calzada, J. Pérez de la Cruz, J. R. A. Fernández, and R. Jiménez, "Morphotropic Phase Boundary in Solution Derived $(Bi_{0.5}Na_{0.5})_{1-x}Ba_xTiO_3$ Thin Films. Part II Functional Properties", *J. Am. Ceram. Soc.* [Epub ahead of print].
[33]S. Hoffmann and R. Waser, "Control of the Morphology of CSD- Prepared $(Ba, Sr)TiO_3$ Thin Films," *J. Eur. Ceram. Soc.*, **19**, 339–43 (1999).
[34]L. Lutterotti, "Materials Analysis Using Diffraction," http://www.ing.unitn.it/~maud/ [accessed on 18 August 2011].
[35]L. Fuentes-Montero, M. E. Montero-Cabrera, and L. Fuentes-Cobas, "The Software Package ANAELU for X-ray Diffraction Analysis Using two-Dimensional Patterns," *J. Appl. Crystallogr.*, **44**, 241–6 (2011).
[36]L. Fuentes-Montero and L. Fuentes-Cobas, "Modelling of Texture Effect on 2d Diffraction Patterns"; SSRL/LCLS User's conference, Standford, CA, 2008.
[37]E. Kotai, "Computer Method for Analysis and Simulation of RBS and ERDA Spectra," *Nucl. Instrum. Methods, Sect. B*, **85**, 588–96 (1994).
[38]M. Mayer, "SIMNRA: Simulation of RBS, ERD and NRA Spectra," SIMNRA version 5.0, Max-Planck-Institut fur Plasmaphysik Garching, Germany, 2002 http://www.rzg.mpg.de/_mam/ [accessed on 15 February 2011].
[39]G. Picht, J. Töpfer, and E. Hennig, "Structural Properties of $(Bi_{0.5}Na_{0.5})_{1-x}Ba_xTiO_3$ Lead-Free Piezoelectric Ceramics," *J. Eur. Ceram. Soc.*, **30**, 3445–53 (2010).
[40]J. E. Daniels, W. Jo, J. Rödel, and J. L. Jones, "Electric-Field-Induced Phase Transformation at a Lead -Free Morphotropic Phase Boundary: Case Study in a $93\%(Bi_{0.5}Na_{0.5})TiO_3$–7%$BaTiO_3$ Piezoelectric Ceramic," *Appl. Phys. Lett.*, **95**, 032904 (2009).
[41]L. Pardo, E. Mercadelli, A. García, K. Brebøl, and C. Galassi C, "Field-Induced Phase Transition and Relaxor Character in Submicrometer Structured Lead-Free $(Bi_{0.5}Na_{0.5})0.94Ba_{0.06}TiO_3$ Piezoceramics at the Morphotropic Phase Boundary," *IEEE Trans. Ultrason. Ferroelectr. Freq. Control*, **58** [9] 1893–904 (2011).
[42]M. L. Calzada, R. Jiménez, A. González, J. García-López, D. Leinen, and E. Rodríguez-Castellón, "Interfacial Effects and Electrical Characteristics of Ferroelectric Strontium Bismuth Tantalate Thin Films on Pt/TiO_2 and Ti/Pt/Ti Heterostructure Electrodes," *Chem. Mater.*, **17**, 1441–9 (2005). □